Enriched Multi-Point Flux Approximation for General Grids

Qian-Yong Chen,[*] Jing Wan,[†] Yahan Yang,[†] and Rick T Mifflin[†]

Abstract

It is well known that the two-point flux approximation, a numerical scheme used in most commercial reservoir simulators, has $O(1)$ error when grids are not $\mathbf{K}$-orthogonal. In the last decade, multi-point flux approximations have been developed as a remedy. However, non-physical oscillations can appear when the anisotropy is really strong. We found out the oscillations are closely related to the poor approximation of pressure gradient in flux computation.

In this paper, we propose the control volume enriched multi-point flux approximation (EMPFA) for general diffusion problems on polygonal and polyhedral meshes. Non-physical oscillations are not observed for realistic and strongly anisotropic heterogeneous material properties described by a full tensor. Exact linear solutions are recovered for grids with non-planar interfaces, and a first and second order convergence are achieved for the flux and scalar unknowns respectively.

Keywords: Anisotropy, Control volume, Heterogeneous, Full tensor diffusion, MPFA

---

[*]Postdoctoral associate at Institute for Mathematics and its Applications, University of Minnesota. Partially funded by ExxonMobil Upstream Research Company. Current address: Department of Mathematics and Statistics, University of Massachusetts Amherst (qchen@math.umass.edu).

[†]ExxonMobil Upstream Research Company, Houston, TX.

1

1   Introduction

Many physical processes, for example the Darcy flow in porous media and the heat transfer in Basin modeling, can be modeled by a diffusion equation in the form

$$-\nabla \cdot \mathbf{K} \nabla p = f. \tag{1}$$

The diffusion coefficient $\mathbf{K}$ is often a space dependent full tensor because of the strongly anisotropic and inhomogeneous media, which imposes a great challenge for numerical schemes, especially when the principle directions of $\mathbf{K}$ are not aligned with the grids. This is usually the case for unstructured meshes. In the following, we will state everything in the context of reservoir simulation, simply because the initial motive is to develop a more robust discretization for simulating multi-phase flow in porous media, although the proposed scheme can apply to general diffusion problems described by (1). In this paper, we assume $\mathbf{K}$ is a piecewise constant tensor. The scalar unknown p will be called pressure for convenience.

There have been extensive research on developing numerical schemes for Eq. (1) on general grids. Some highly desirable properties of the discretization beyond the classical stability and accuracy, include local mass conservation, harmonic average transmissibilities, discrete maximum principle, and cost-effective. For historic reasons, the two-point flux approximation (TPFA), a scheme that is inconsistent when the grids are not $\mathbf{K}$-orthogonal, is still used in most commercial reservoir simulators. Roughly speaking, $\mathbf{K}$-orthogonality means the flux $-\mathbf{K}\nabla p \cdot \mathbf{n}$ can be approximated by a factor of the pressure difference from two neighbouring control volumes (see (8) for one example). Unfortunately, $\mathbf{K}$-orthogonality is often lost in the grids that honor the geologic features such as sloping faults and channels, and other important features such as nearly horizontal wells [17]. Recently, Wu and Parashkevov studied the effect of non-orthogonality error of deviated grids on the flow solutions from the two-point flux, control volume method [32]. They concluded that for most practical cases the errors in horizontal flow are relatively small and the errors in vertical flow can be rather significant.

To obtain a consistent scheme, different groups of researchers have independently developed

the so-called control volume multi-point flux approximation (MPFA), such as Aavatsmark et al [3], Edwards and Rogers [14], Verma and Aziz [31]. Since their pioneer work, a whole class multi-point flux methods have been developed [2]. In [21], the authors implement the multi-point flux methods on a hexahedral grid. More recently, Klausen and Russell [18] compare the multi-point flux approximation with other locally conservative schemes which handle discontinuous coefficients, such as the classical mixed finite element method and the support operators method (also called mimetic finite difference method). Klausen and Winther also proved the convergence of multi-point flux approximations on smooth quadrilateral grids [19].

In most cases, good results are obtained by multi-point flux methods, but non-physical oscillations can appear for strongly anisotropic fields because of non-monotonicity of the matrix (see, e.g., [23, 25]). That means the numerical solution does not satisfy the maximum principle, although the analytical solution does. In order to improve the monotonicity property, Nordbotten and Eigestad recently developed a MPFA Z-method for quadrilateral grids by choosing a different stencil when computing the flux [26]. But it is not clear how to extend their method to unstructured polyhedral meshes. Other very recent research on this issue includes the reduced integration of mixed finite element method [22] and the corner velocity interpolation method [16].

The mimetic finite difference schemes proposed by Shashkov et al [30] are very promising in terms of dealing with highly distorted grids and heterogeneous media. The convergence and super convergence [5, 6] are also established for smooth problems on smooth meshes by rewriting it into the form of mixed finite element methods. (A more general proof was provided in [7].) Furthermore, in [8] Brezzi et al employ an innovative technique to generalize it to a family of schemes with parameters which might be tuned to achieve the discrete maximum principle. But by now such a scheme still does not exist, and the computational cost of mimetic finite difference schemes is an issue too.

There is also considerable advance in mixed finite element type methods for distorted general meshes [9, 11], but they are quite expensive and 3-D case is still under development [24, 20]. A worthy alternative, the control volume finite element (CVFE) methods (often called finite volume

element methods) [4, 10, 29], are locally mass conservative and applicable on flexible grids, but they do not handle discontinuous diffusion coefficients well [13].

In this paper, we develop a new multi-point flux approximation method, called enriched multi-point flux approximation (EMPFA), based on more consistent pressure approximations in the inter-action region. The proposed method does not produce oscillatory solutions and works for general matching or nonmatching polygonal and polyhedral meshes, including meshes with non-planar interfaces. Expected convergence rate is also achieved for the new method, Moreover, the enriched multi-point flux approximation is equivalent to the two-point flux approximation for $\mathbf{K}$-orthogonal grids.

The remaining of the paper is organized as follows. In Sec. 2, we restate the original multi-point flux approximation on quadrilateral grids. Section 3 describes our new multi-point flux approximation for two-dimensional grids, shows its numerical convergence, and compares the numerical results with the multi-point flux approximation method. In section 4, we extend the technique in Sec. 3 to polyhedral meshes. Finally, we summarize the paper and make some concluding remarks in Sec. 5.

2   Multi-Point Flux Approximation

In this section, we first briefly review the multi-point flux method with surface mid-points as continuity points (called O-method [2]) on quadrilateral grids. The extension to unstructured grids is trivial. Then we analyze the limitations of the MPFA O-method.

2.1   Description of Multi-Point Flux Approximation

Let $\Omega \in R^2$ be the computational domain, and divide it into non-overlapping quadrilateral control volumes $\Omega = \cup V_i$. Consider Eq. (1) with piecewise constant permeability $\mathbf{K}$ (i.e., constant on each V_i). In control volume multi-point flux approximation methods, the mass is conserved on each control volume, i.e., integrate the equation on control volumes $\{V_i\}$ to obtain

$$-\int_{\partial V_i} \mathbf{K}\nabla p \cdot \mathbf{n} \, dS = \int_{V_i} f \, dV, \qquad \forall V_i, \tag{2}$$

where the left hand side is the amount of flux (i.e., $-\mathbf{K}\nabla p \cdot \mathbf{n}$) across the boundary of V_i.

In MPFA method, there is only one degree-of-freedom (usually pressure at the mass center) for each control volume. The fluxes across control volume interfaces are computed for each interaction region and expressed in terms of those degrees-of-freedom. When computing the fluxes, each interface (a line segment) is divided into two parts, on which the fluxes are first computed separately and then summed up to be the flux across the whole interface. For example, Figure 1 shows four control volumes with centers C_i's which meet at point O. The polygon area formed by cell centers C_i's and edge middle points M_i's is called *interaction region*. The small quadrilateral of each control volume included in the interaction region is called *sub-volume*, e.g., $M_1OM_4C_1$. (Note that each vertex of the mesh corresponds to an interaction region.) In this region, only the fluxes across half edges OM_i's will be computed. Then we loop over all the interaction regions to compute the fluxes for all the control volume boundaries/interfaces.

In order to compute the fluxes across OM_i's (i.e., the integral of $-\mathbf{K}\nabla p \cdot \mathbf{n}$ on OM_i), the values of p at M_i's are introduced as four temporary unknowns. The method with this choice is called MPFA O-method. (One could also use the values of p at other points as the temporary unknowns.)
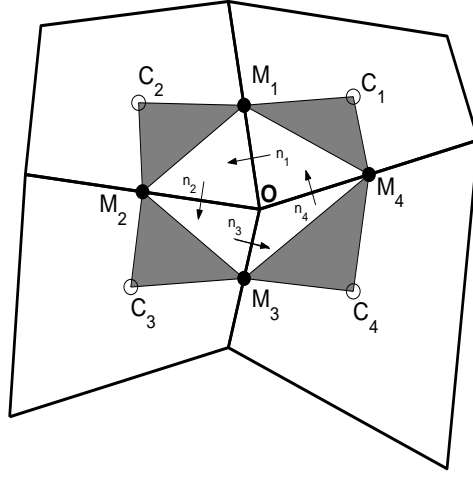
Figure 1: Multi-point flux method: interaction region

Recall that the primary unknowns are the values of p at C_i's. With both primary and temporary unknowns, we can compute ∇p and then the fluxes by assuming p is a linear function on shaded triangles in Fig. 1. For example, when computing the flux across OM_1 and OM_4 from volume C_1, a constant gradient ∇p is computed from the linear function on $\Delta_{M_1 M_4 C_1}$, and then extrapolated to be the gradient on the whole quadrilateral sub-volume $M_1 O M_4 C_1$. Hence the flux across OM_1 and OM_4 can be written into the form of $\mathbf{a}^T \mathbf{K_1} \nabla p$ with the area vector $\mathbf{a} = |OM_1| \mathbf{n_1}$ and $-|OM_4| \mathbf{n_4}$ respectively, where $\mathbf{K}_1$ is the diffusion tensor on volume C_1.

Denote $\mathbf{P} = (p_{C_1}, p_{C_2}, p_{C_3}, p_{C_4})^T$ and $\bar{\mathbf{P}} = (p_{M_1}, p_{M_2}, p_{M_3}, p_{M_4})^T$, where p_A represents the value of p at point A. Rewrite the fluxes across half edges OM_i's from volume C_i's into a matrix vector product form as $\mathbf{A}\bar{\mathbf{P}} + \mathbf{B}\mathbf{P}$, and the fluxes from the opposite volumes as $\mathbf{C}\bar{\mathbf{P}} + \mathbf{D}\mathbf{P}$. The formula for matrices $\mathbf{A}, \mathbf{B}, \mathbf{C}, \mathbf{D}$ can be found in [2]. Balancing the flux across OM_i's from both sides yields

$$\mathbf{A}\,\bar{\mathbf{P}} + \mathbf{B}\,\mathbf{P} = \mathbf{C}\,\bar{\mathbf{P}} + \mathbf{D}\,\mathbf{P}.$$

From the above equation, $\bar{\mathbf{P}}$ can be solved in terms of $\mathbf{P}$, and then substituted back to the flux expression. In the end, the fluxes across the half edges can be written as

$$\mathbf{TP} = [\mathbf{A}(\mathbf{A} - \mathbf{C})^{-1}(\mathbf{D} - \mathbf{B}) + \mathbf{B}]\mathbf{P},$$

where the matrix $\mathbf{T}$ is called transmissibility matrix in petroleum industry.
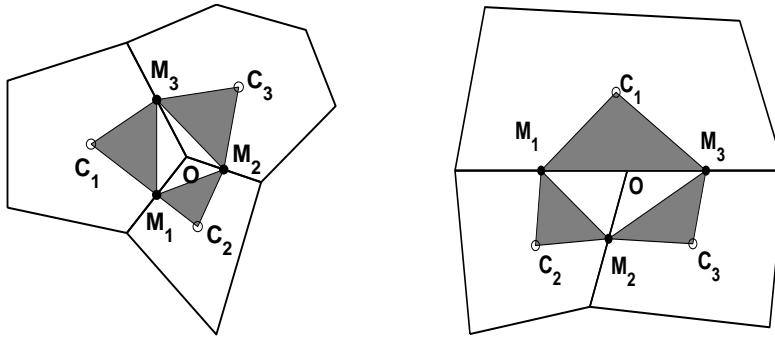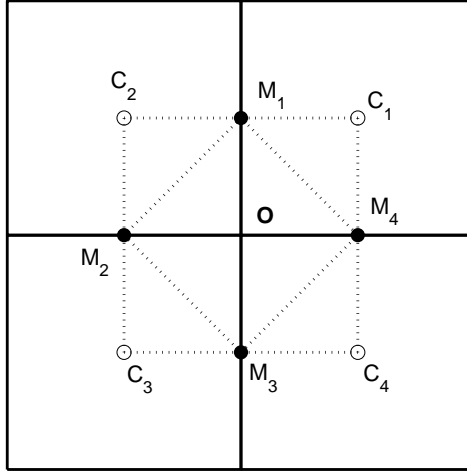
Figure 2: General two-dimensional grids

Figure 3: An interaction region of rectangular control volumes.

Note that the MPFA-O method also applies to both matching and non-matching unstructured polygon grids as shown in Fig. 2, although the above description is only for quadrilateral meshes.

2.2 Limitations of MPFA O-Method

In most cases, good results are obtained from the multi-point flux methods. However, non-physical oscillations can appear when the anisotropy of permeability field is strong (see Sec. 3.4 or [23, 25]). Most researchers agree that the oscillations are due to the non-monotonicity of the matrix. In the following, we do a non-rigorous analysis from the aspect of accuracy, which leads to the development of our new multi-point flux method in the next section.

Consider an interaction region of rectangular control volumes as shown in Fig. 3. As described in the previous section, a linear pressure is assumed on $\Delta_{M_1 M_4 C_1}$ in the multi-point flux approxi-

mation method. It yields a constant pressure gradient as

$$\begin{cases} u &= \frac{p_{C_1} - p_{M_1}}{\Delta x}, \\ v &= \frac{p_{C_1} - p_{M_4}}{\Delta y}, \end{cases}$$

in which Δx and Δy are the grid-size in x and y-direction. This pressure gradient is then extrapolated to the whole quadrilateral $M_1 O M_4 C_1$ and used to compute the flux across edges OM_1 and OM_4 from control volume C_1. From the Taylor expansion at point M_1, one can have

$$\left. \frac{\partial p}{\partial y} \right|_{M_1} = v + \Delta x \left. \frac{\partial^2 p}{\partial x \partial y} \right|_{M_1} + O(\Delta y + (\Delta x)^2). \tag{3}$$

Clearly, v will be a poor approximation of $\frac{\partial p}{\partial y}$ at point M_1 if $\frac{\partial^2 p}{\partial x \partial y} \sim \frac{1}{\Delta x}$ in the neighbourhood of M_1. Similar result holds for u being an approximation of $\frac{\partial p}{\partial x}$ at point M_4. We believe that these poor approximations of fluxes due to the built-in extrapolation in MPFA contribute to the non-physical oscillations. If the grid is fine enough in the sense of $\Delta x \frac{\partial^2 p}{\partial x \partial y}$ being small near point M_1, the oscillation should be less severe. It is confirmed by the first example in Sec. 3.4.

Note that these poor approximations do NOT come into the formulation of fluxes when the grid is **K**-orthogonal. It explains why no oscillation was observed for **K**-orthogonal grids.

3   Enriched Multi-Point Flux Approximation on Polygon Meshes

In this section, we present a new multi-point flux approximation, called enriched multi-point flux approximation. It works for general polygon meshes like the multi-point flux approximation, but all the descriptions and explanations are only for quadrilateral control volumes, with straightforward extension to unstructured grids. All the notations will be the same as those in Sec. 2 if not specified otherwise.

3.1   Description

The enriched multi-point flux approximation method follows the same framework as the MPFA O-method: introducing some temporary unknowns in the beginning in order to compute the gradient of p, and then eliminating them by balancing fluxes. But in the EMPFA method we include one more temporary unknown, p at the 'center' of interaction region, to avoid the extrapolation procedure in the MPFA method which has been previously shown to contribute to the non-physical oscillations.

We propose two different approximation for the scalar unknown p. As shown in the left of Fig. 4, the first approximation is a piecewise linear function which is linear on each triangle (e.g., M_1OC_1). Note that only the interaction region is drawn. The second option is to approximate p with a piecewise bilinear function on each quadrilateral in the right of Fig. 4. The bilinear interpolation is included in **Appendix** A for completeness. With either approximation for p, we compute the fluxes across edges OM_i's and balance them to get a system of four equations written as

$$\mathbf{A}\,\bar{\mathbf{P}} + \mathbf{B}\,\mathbf{P} + p_O \cdot \vec{\mathbf{l}} = \mathbf{C}\,\bar{\mathbf{P}} + \mathbf{D}\,\mathbf{P} + p_O \cdot \vec{\mathbf{r}}. \tag{4}$$

Note that matrices $\mathbf{A}, \mathbf{B}, \mathbf{C}, \mathbf{D}$ may have different entries from those in Sec. 2. For simplicity, the explicit formula for vectors $\vec{\mathbf{l}}$ and $\vec{\mathbf{r}}$ are not given. The new temporary unknown p_O, the value of p at point O, comes into the formulation of fluxes as a result of approximating p in a richer space (compared to the multi-point flux approximation). When the bilinear approximation is chosen, the gradient of p is not a constant on the half edges OM_i's except for some special grids. In this case,
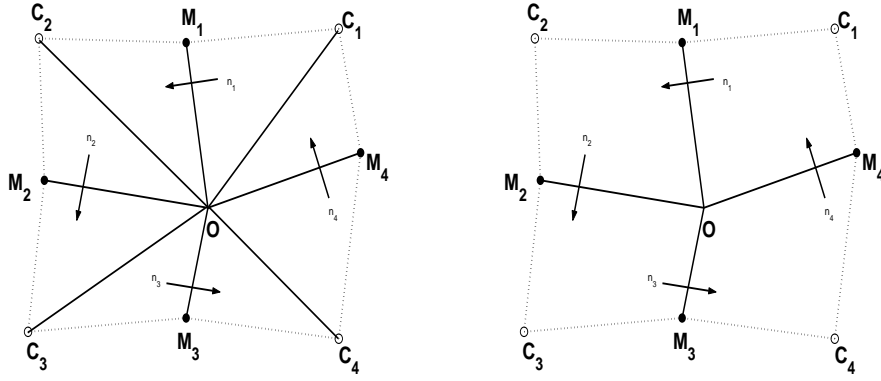
9

Figure 4: EMPFA interaction region. Left: piecewise linear approximation; Right: piecewise bilinear approximation.

a single point quadrature (e.g. M_i) can be used to compute the integral of flux on the half edges.

In order to eliminate all the five temporary unknowns, one more equation besides Eq. (4) is needed. We propose two different ways to obtain the extra equation.

The first approach is to solve Eq. (1) on a small volume surrounding the interaction region center. We only describe this approach with bilinear approximations of pressure p. The procedure is similar for the piecewise linear approximation. In Fig. 5, $\Omega_\epsilon = D_1 D_2 D_3 D_4$ with $|OD_i| = \epsilon|OM_i|$ is the small volume on which Eq. (1) will be solved, where ϵ is a small positive number. So,

$$-\int_{\partial\Omega_\epsilon} \mathbf{K}\nabla p \cdot \mathbf{n} \, dS = \int_{\Omega_\epsilon} f \, dV, \tag{5}$$

where $\partial\Omega_\epsilon = D_1 D_2 \cup D_2 D_3 \cup D_3 D_4 \cup D_4 D_1$. Be aware that only the small volume for piecewise bilinear approximation is plotted in Fig. 5.

Consider edge $D_4 D_1$. After obtaining the bilinear transformation coefficients for the quadrilateral $M_1 O M_4 C_1$ as described in **Appendix** A, the flux across edge $D_4 D_1$ can be computed as

$$-\epsilon \cdot \frac{1}{a_2 b_3 - a_3 b_2} \begin{pmatrix} b_3 - b_2 & a_2 - a_3 \end{pmatrix} \mathbf{K_1} \begin{pmatrix} b_3 & -b_2 \\ -a_3 & a_2 \end{pmatrix} \begin{pmatrix} -1 & 1 & 0 & 0 \\ -1 & 0 & 0 & 1 \end{pmatrix} \begin{pmatrix} p_{M_1} \\ p_O \\ p_{M_4} \\ p_{C_1} \end{pmatrix} + O(\epsilon^2). \tag{6}$$

In the same way, we compute the flux across other edges of $\partial\Omega_\epsilon$. Therefore, the left hand side of Eq. (5) is equal to

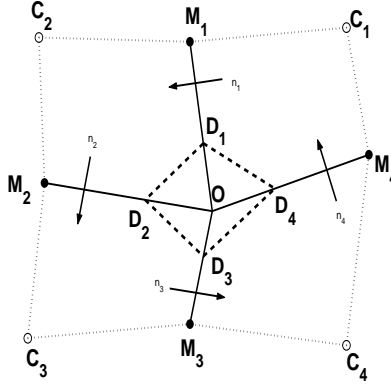$$\epsilon \, g(p_O, \mathbf{P}, \bar{\mathbf{P}}) + O(\epsilon^2), \tag{7}$$

10

Figure 5: EMPFA interaction region: a small volume.

with the explicit expression of g being computed from the sum of (6) for all Ω_ϵ edges.

Now we consider the right hand side of Eq. (5). Assume f is a square integrable function on a volume $\tilde{\Omega} \supset \Omega_\epsilon$ for some $\epsilon > 0$, i.e.,

$$\left(\int_{\tilde{\Omega}} |f|^2 \, dV \right)^{1/2} < \infty.$$

By the dominated convergence theorem [28], we have

$$\left(\int_{\Omega_\epsilon} |f|^2 \, dV \right)^{1/2} \to 0 \qquad \text{as} \qquad \epsilon \to 0.$$

Rewrite it into the standard asymptotic notation

$$\left(\int_{\Omega_\epsilon} |f|^2 \, dV \right)^{1/2} = o(\epsilon^0).$$

According to Schwarz inequality, we have

$$\left| \int_{\Omega_\epsilon} f \, dV \right| \le \left(\int_{\Omega_\epsilon} |f|^2 \, dV \right)^{1/2} \cdot \left(\int_{\Omega_\epsilon} 1 \, dV \right)^{1/2} = o(\epsilon).$$

Combining the above equation with (7), one can have

$$\epsilon \, g(p_O, \mathbf{P}, \bar{\mathbf{P}}) + O(\epsilon^2) = o(\epsilon).$$

Let $\epsilon \to 0$ to obtain the final equation

$$g(p_O, \mathbf{P}, \bar{\mathbf{P}}) = 0,$$

from which we can solve p_O in terms of $\mathbf{P}$ and $\bar{\mathbf{P}}$. Then we can compute the flux by solving $\bar{\mathbf{P}}$ in terms of $\mathbf{P}$ in the same way as in the multi-point flux approximation.

11

Remark 1 *The resultant equation is in some sense independent of the shape of Ω_ϵ because of the limiting process. One may be able to eliminate p_O without letting $\epsilon \to 0$. But the formulation will not be as neat as the one we get here.*

Remark 2 *Although we state our algorithm for an interaction region with four sub-volumes, it works for any interaction region from general two-dimensional grids.*

The second approach is to solve the original equation (i.e., Eq. (1)) on the whole interaction region with the standard Finite Element Method (FEM). The mesh can be either one in Fig. 4, depending on which approximation is used for p. Dirichlet boundary conditions are imposed, and a linear p is interpolated from its values at two ending points for each boundary line segment connecting C_i's and M_i's. From this FEM solve, the extra unknown p_O can be expressed as a linear function of $\bar{\mathbf{P}}$ and $\mathbf{P}$, which is then plugged into Eq. (4) to eliminate all the other temporary unknowns. After the elimination, the fluxes will be functions of primary unknowns only, like those in the multi-point flux approximation methods.

One can combine the linear or bilinear approximation with either approach to obtain the extra equation. Almost equivalent numerical results were obtained for the two different approximations.

Note that the enriched multi-point approximation method works for both matching and non-matching unstructured polygon grids. In the following, we show how to make our algorithm work for non-matching grids.

3.2   Non-Matching Grids

When a linear pressure is assumed, the enriched multi-point flux approximation automatically works for non-matching grids. Only for bilinear pressure interpolation we need to make a minor change of the above algorithm. Consider a typical interaction region with non-matching grid point as shown in Fig. 6. Since $C_1 M_1 O M_3$ is a degenerated quadrilateral, the point O will be a singularity point if we still use bilinear transformation to map it to a standard square element. So instead of treating $C_1 M_1 O M_3$ as one sub-volume, we decompose it into two triangles: $\Delta C_1 M_1 O$ and $\Delta C_1 O M_3$, on each of which a linear interpolation is applied. Then following the procedure
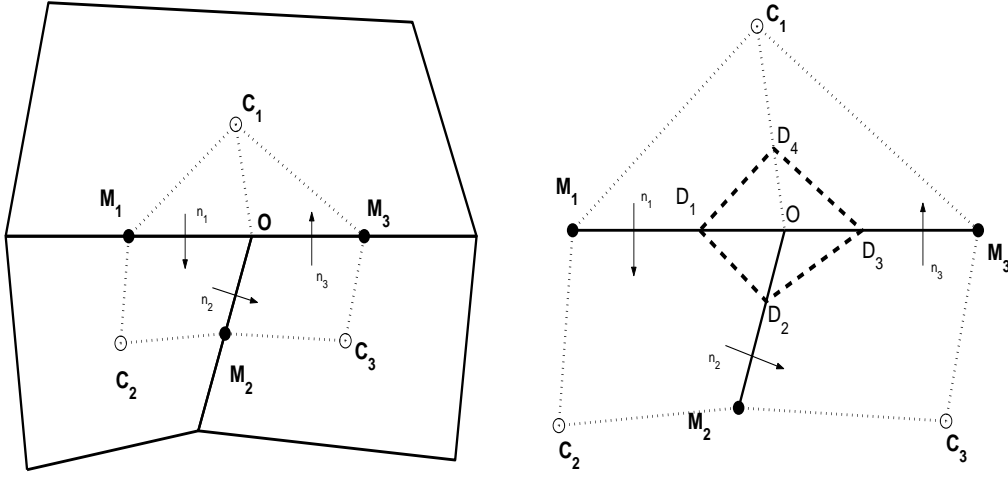
Figure 6: Interaction region with non-matching grid point. $|OD_i| = \epsilon|OM_i|, i = 1, 2, 3; |OD_4| = \epsilon|OC_1|$.

described in the previous sections, we can compute the flux across all the edges in the interaction region. The small volume used to generate the extra equation to eliminate p_O is shown on the right part of Fig. 6.

3.3 Equivalence of EMPFA and TPFA for K-Orthogonal Grids

Here we show the enriched multi-point flux approximation is equivalent to the conventional two-point flux approximation for **K**-orthogonal grids.

Consider the flux across edge M_1O from volume C_1 in Fig. 5. Note that point M_1 has coordinate $(0, 0)$ in ξ-η coordinate system (see **Appendix** A). Using the formula given in **Appendix** A, the pressure gradient at point M_1 is

$$\frac{1}{a_2 b_3 - a_3 b_2} \begin{pmatrix} b_3 & -b_2 \\ -a_3 & a_2 \end{pmatrix} \begin{pmatrix} -1 & 1 & 0 & 0 \\ -1 & 0 & 0 & 1 \end{pmatrix} \begin{pmatrix} p_{M_1} \\ p_O \\ p_{M_4} \\ p_{C_1} \end{pmatrix}.$$

Since the grid is **K**-orthogonal, there exists a constant c such that

$$\mathbf{a}^T \mathbf{K} = c \, \overrightarrow{C_1 M_1} = c \left(-a_3 \quad -b_3 \right). \tag{8}$$

Plug the above two equations into the flux formula $\mathbf{a}^T \mathbf{K} \nabla p$ to obtain

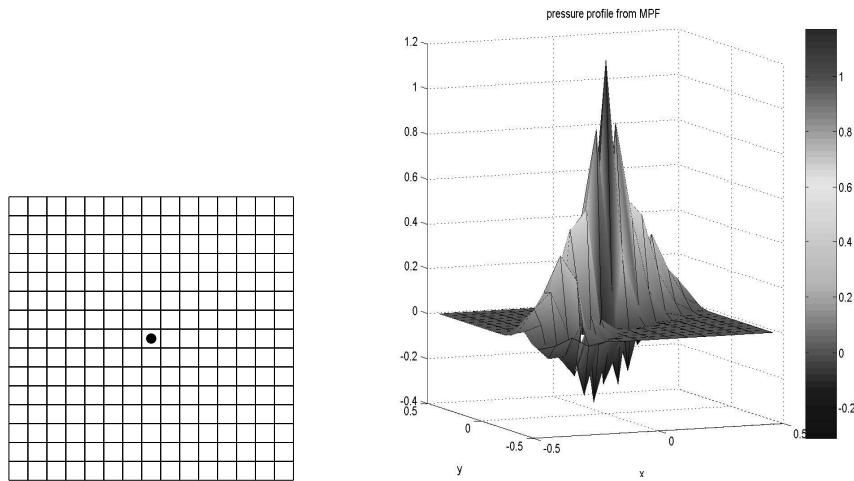$$\mathbf{a}^T \mathbf{K} \nabla p = c \, (p_{M_1} - p_{C_1}),$$

13

Figure 7: Oscillatory solution from MPFA on quadrilateral control volumes. $k_1 = 1, k_2 = 1000, \theta = \pi/3$. Left: grid of size 15×15; Right: pressure profile.

which is exactly the same formula as that from the two-point flux approximation. Therefore we have showed that the enriched multi-point flux approximation is equivalent to the conventional two-point flux approximation for **K**-orthogonal grids.

3.4 Numerical Experiments

In this section, we solve Eq. (1) for various permeabilities and solutions with different regularities.

3.4.1 Non-Physical Oscillations

The problem described in [23] is to solve Eq. (1) with permeability

$$\mathbf{K} = \begin{pmatrix} \cos\theta & \sin\theta \\ -\sin\theta & \cos\theta \end{pmatrix} \begin{pmatrix} k_1 & 0 \\ 0 & k_2 \end{pmatrix} \begin{pmatrix} \cos\theta & -\sin\theta \\ \sin\theta & \cos\theta \end{pmatrix}. \tag{9}$$

The computation domain is $[-0.5, 0.5] \times [-0.5, 0.5]$ with a well sitting in the middle. Constant pressure is used as boundary conditions. A constant flow rate is specified in the code for the control volume including the well. As shown in Fig. 7 and Fig. 8, non-physical oscillations are present when k_2/k_1 is large and the grid is not **K**-orthogonal. Figure 9 shows the solution from the multi-point flux approximation on finer quadrilateral grids. Clearly the oscillation becomes less severe when refining the grid.
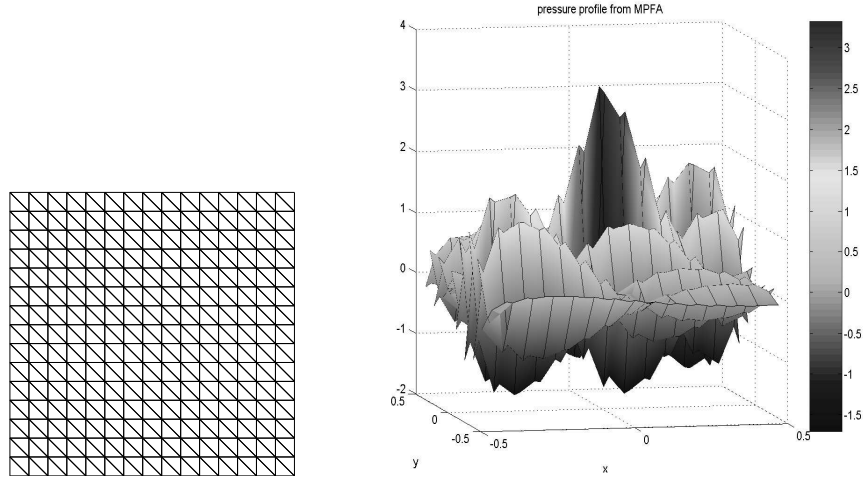
14

Figure 8: Oscillatory solution from MPFA on triangular control volumes. $k_1 = 1, k_2 = 25, \theta = \pi/3$. Left: grid; Right: pressure profile.
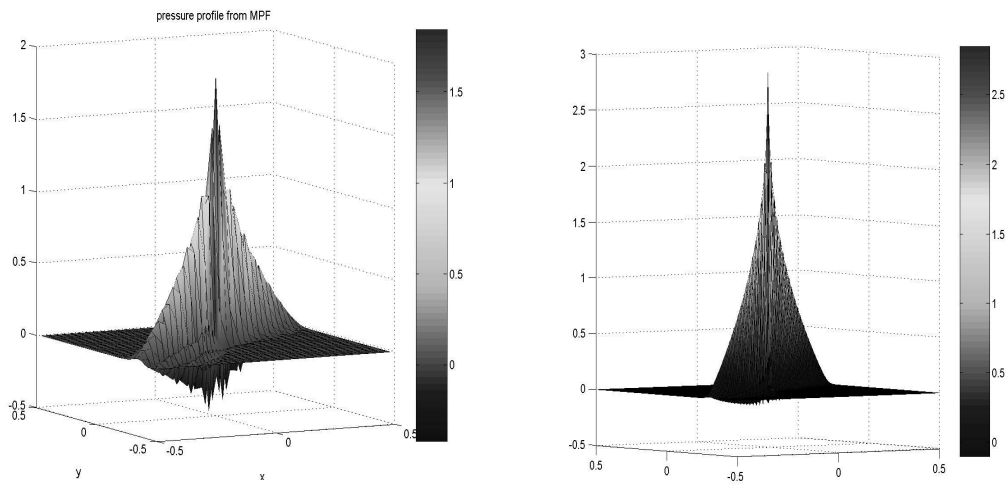

Figure 9: Less oscillatory solution from MPFA on finer quadrilateral grids. $k_1 = 1, k_2 = 1000, \theta = \pi/3$. Left: 33×33; Right: 99×99.
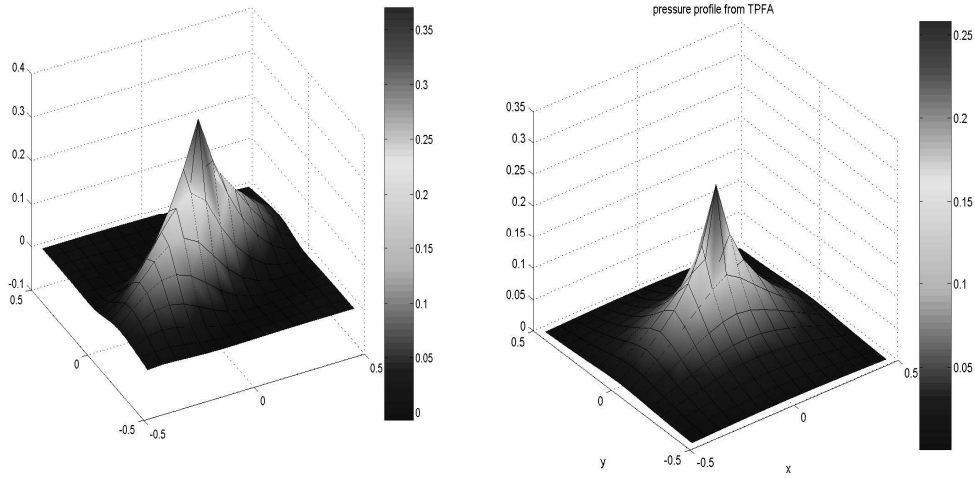
Figure 10: Pressure profile on the quadrilateral grid. Left: EMPFA. Right: TPFA. $k_1 = 1, k_2 = 1000, \theta = \pi/3$. Grid: 15×15.

Figures 10 and 11 display the solution from the enriched multi-point flux approximation. No oscillation is observed. For comparison purpose, we also show the pressure profile from the two-point flux approximation. The anisotropic structure of the pressure profile is clearly distorted by the two-point flux approximation.

In order to have a quantitative comparison between the EMPFA and MPFA methods, we consider a case similar to the above problem. Assume the analytical solution is $p(x, y) = -q \log(r) + c$, where $r = \sqrt{\xi^2 + \eta^2}$ with

$$\begin{pmatrix} \xi \\ \eta \end{pmatrix} = \begin{pmatrix} \frac{1}{\sqrt{k_1}} & \\ & \frac{1}{\sqrt{k_2}} \end{pmatrix} \begin{pmatrix} \cos\theta & -\sin\theta \\ \sin\theta & \cos\theta \end{pmatrix} \begin{pmatrix} x \\ y \end{pmatrix}.$$

The constants q and c are chosen such that $p \geq 0$ on the computational domain $[-0.5, 0.5] \times [-0.5, 0.5]$. The permeability tensor is assumed to have the form as given in Eq. (9). Exact solution is applied as Dirichlet boundary conditions. From the result shown in Fig. 12, the enriched multi-point flux method is more accurate than the original multi-point flux method for this test case.

3.4.2 Uniform Flow

The analytical solution is a uniform flow on $[-0.5, 0.5] \times [-0.5, 0.5]$. Specially, we choose

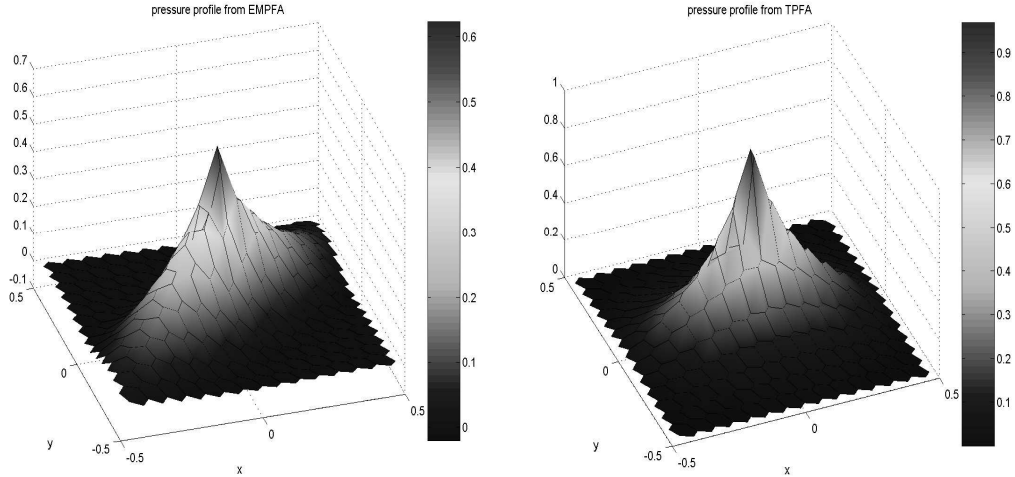$$p(x, y) = x + 4, \qquad \text{and} \qquad p(x, y) = y + 2.$$

16

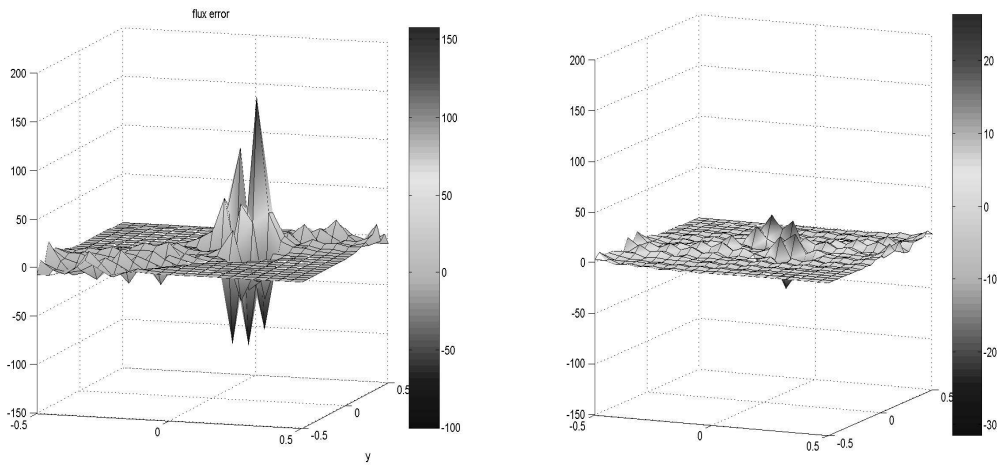Figure 11: Pressure profile on the triangular grid. Left: EMPFA. Right: TPFA. $k_1 = 1, k_2 = 25, \theta = \pi/3$.

Figure 12: Flux error. Left: MPFA; Right: EMPFA. $k_1 = 1, k_2 = 1000, \theta = \pi/3$. Quadrilateral grid of size 11×11.
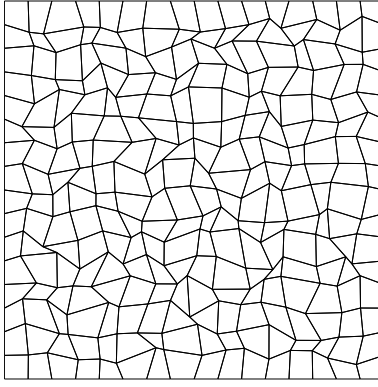
Figure 13: Random grid.

The permeability is assumed to be a diagonal tensor, $\mathbf{K} = diag(10, 1)$. The computation is done on a pseudo-random grid in Fig. 13. The grid is generated by first building a uniform Cartesian grid and then perturbing it in a certain way such that all the control volumes are still convex quadrilateral. More details on construction of this type of random grids can be found in [30]. As expected, the exact solution is recovered by the enriched multi-point flux method.

3.4.3 Convergence Study

We now study the convergence rate of the enriched multi-point flux approximation. The discrete L_2 error of pressure and flux take the form

$$
\begin{cases}
ep & = \left(\sum_i |V_i| \, (p_{ex,i} - p_i)^2\right)^{1/2}, \\
ef & = \left(\sum_{e\in\mathcal{E}} Q_e \left(\frac{f_{ex,e} - f_e}{|e|}\right)^2 \Big/ \sum_{e\in\mathcal{E}} Q_e\right)^{1/2},
\end{cases}
$$

where $\{V_i\}$ is the set of all the control volumes and $\mathcal{E}$ is the set of all the control volume edges. $|V_i|$ denotes the volume (area for 2D problems) of control volume V_i, while Q_e is the volume associated with edge e. In this paper, the sum of the area of sub-volumes sharing edge e is used as Q_e. The same discrete error measure has been used in [18] and [15].

Example 1: The analytical solution $p(x, y) = \cos(\pi x)\cos(\pi y) + 2$ and $\mathbf{K} = diag(10, 1)$. The computation is done on the random grid as shown in Fig. 13. During the grid refinement, we first refine the Cartesian mesh uniformly and then perturb the mesh to obtain a finer random grid. As shown in Tab. 1, the expected convergence rate is achieved for the enriched multi-point flux
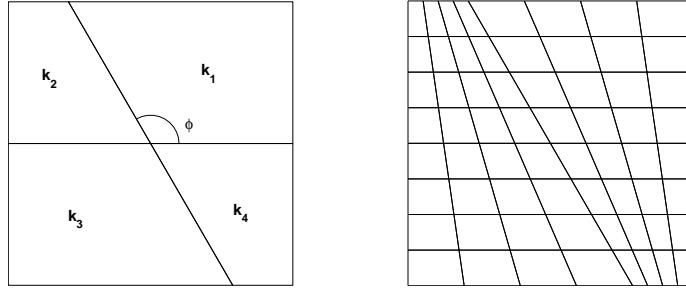
18

Figure 14: Discontinuous permeability field. Left: the computation domain; Right: 8×8 mesh which honors discontinuity of permeability.

method.

Table 1: Convergence rate. $p(x, y) = \cos(\pi x)\cos(\pi y) + 2$ and $\mathbf{K} = diag(10, 1)$.

N	EMPFA				MPFA			
	ep	Rate	ef	Rate	ep	Rate	ef	Rate
8	0.01593		1.4039		0.01892		1.7415	
16	0.00344	2.21	0.6198	1.18	0.00369	2.36	0.7691	1.18
32	0.00082	2.06	0.2702	1.20	0.00100	1.88	0.3851	1.00
64	0.00023	1.81	0.1195	1.18	0.00029	1.78	0.1835	1.07

Example 2: Consider a case with discontinuous permeability field. Figure 14 shows the domain including four sub-domains each of which is assumed to have homogeneous isotropic permeability field, i.e., $\mathbf{K_i} = k_i\mathbf{I}$. The four sub-domains meet at the center (origin $(0, 0)$) with angle ϕ. We seek an analytical solution with form

$$p(x, y) = p(r, \theta) = r^\alpha(a_i \sin(\alpha\theta) + b_i \cos(\alpha\theta)), \quad \text{if } (x, y) \in i^{\text{th}} \text{ sub-domain}, \qquad i = 1, \cdots, 4,$$

in the polar coordinate system. The coefficients a_i's, b_i's and α can be computed from the continuity conditions of pressure p and flux $\mathbf{K}\nabla p \cdot \mathbf{n}$ across the interfaces of sub-domains. When $k_1 = 100, k_2 = 1, k_3 = 1, k_4 = 1, \phi = 2\pi/3$, we have a solution with

$$\alpha = 0.7547,$$

$$a_1 = 1.00995, \quad a_i = 1.99990, \quad i = 2, 3, 4,$$

$$b_1 = 1, \qquad b_i = 100.98019, \quad i = 2, 3, 4.$$

19

Table 2 lists convergence rates from the enriched multi-point flux method and the multi-point flux method. The order of the L_2 error of pressure is almost $h^{2\alpha}$, which is the optimal rate for conforming finite element methods. (The order $h^{2\alpha}$ is obtained in [27] with the discontinuous Galerkin method.) We also did the test cases with $\phi = \pi/2, k_1 = k_3 = 1, k_2 = k_4 = 5, 10, 100$ as Eigestad and Klausen did in [15]. Similar results were obtained for the enriched multi-point flux approximation.

Table 2: Convergence rate. Permeability $\mathbf{K}_i = k_i\mathbf{I}$ with $k_1 = 100, k_2 = 1, k_3 = 1, k_4 = 1$. $\phi = 2\pi/3$.

N	EMPFA				MPFA			
	ep	Rate	ef	Rate	ep	Rate	ef	Rate
8	0.2688		6.5372		0.3360		4.9486	
16	0.1044	1.36	4.1590	0.65	0.1255	1.42	3.1238	0.66
32	0.0393	1.41	2.5827	0.69	0.0454	1.47	1.9380	0.69
64	0.0145	1.44	1.5803	0.71	0.0162	1.49	1.1877	0.71

3.4.4 Discussion

Thorough numerical tests have been done to verify the accuracy of the enriched multi-point flux approximation method. In the above numerical experiments, almost equivalent results have been obtained for both Dirichlet and Neumann boundary conditions, and for any combination of linear/bilinear pressure approximation and either way to get the extra equation (cf Sec. 3.1). Figures 15-16 list a few other meshes we have tried, some of which are actually exported from the gridding software currently used in ExxonMobil Upstream Research Company. For all the meshes, the exact linear solution can be recovered, and expected convergence is achieved for both the scalar and flux unknowns.

We have also done extensive tests on the robustness of the new method. No oscillations were observed in all the numerical solutions when strongly anisotropic $\mathbf{K}$ exists, except for one case a spike appears in the interior domain. In this particular case, the material property (permeability field) is taken from an XZ cross-section of SPE10 [1]. Then we rotate the permeability for 60 de-
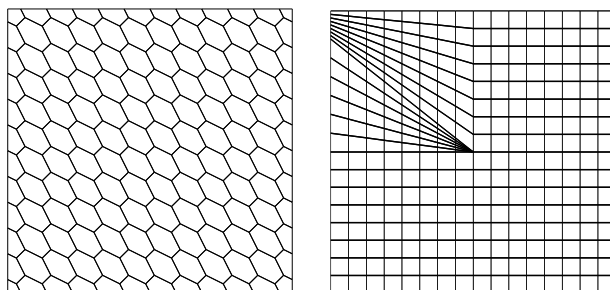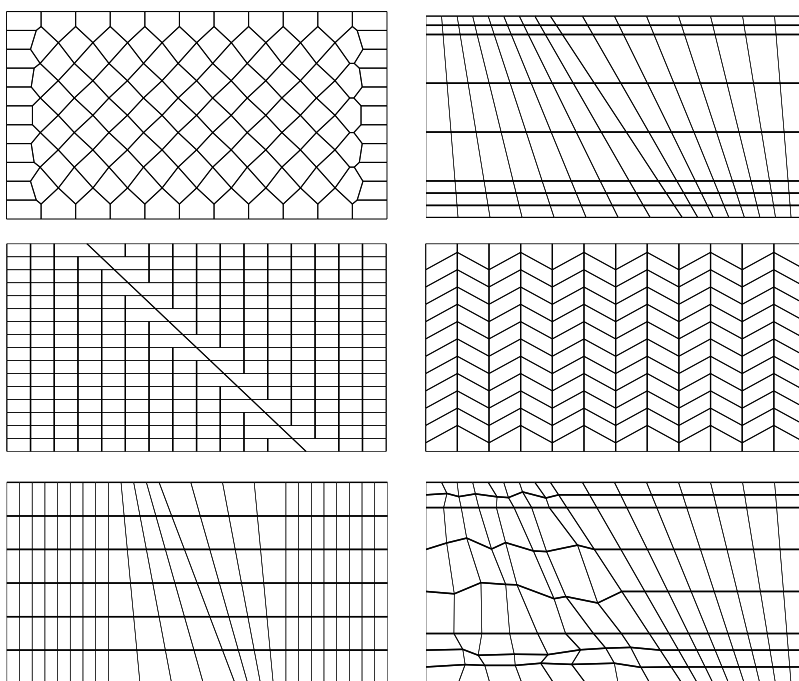
Figure 15: Two dimensional meshes I.

Figure 16: Two dimensional meshes II.

grees, and use the rotated permeability as $\mathbf{K}$ in the numerical experiment. However, the numerical permeability field is not considered to be realistic or physical because the correlation is completely lost after the artificial rotation. Not surprisingly, the control volume finite element method performs much better in this case because it is essentially a finite element method which usually does not have problem with oscillations.

4 Enriched Multi-Point Flux Approximation for Polyhedral Meshes

In this section, we extend the enriched multi-point flux approximation method to three-dimensional grids. For simplicity, we only describe the extension with the combination of piecewise linear approximation of pressure and the FEM way of obtaining the extra equation to eliminate the temporary unknown which sits in the 'center' of the interaction region.

4.1 Local Mesh

From the description in Sec. 3.1, the interaction region in 2D, more precisely every sub-volume, has to be divided into triangles (see Fig. 4) in order to define a piecewise linear approximation for p. Recall that every sub-volume is the portion of one control volume which is inside the interaction region. For two-dimensional grids, each sub-volume is always a quadrilateral except for the non-matching grids (see e.g., Fig. 6). For unstructured polyhedral grids, the sub-volumes are much more complex, and so are the interaction regions. We first need to divide the interaction regions of three-dimensional meshes into tetrahedrons in order to define a piecewise linear approximation for the scalar unknown p.

Since each sub-volume will be partitioned into tetrahedrons separately, we only explain how to divide one sub-volume. Figures 17 - 18 demonstrate the whole process of constructing the sub-volume and local mesh for one particular control volume. Suppose point A is the 'center' of the interaction region, where the control volumes meet. The sub-volume for this control volume is the polyhedron formed by point A, volume center C, and the centers of the control volume faces and edges which meet at point A. In the graph, the face centers (e.g., B) and edge centers (e.g., D and E) are the dark dots and star-shaped points respectively. Note that the control volume faces could be non-flat. In the implementation, we simply use the average of face vertices as the face center for each face.

Half of the sub-volume faces (e.g., $ADBE$) will be shared with another sub-volume. So when dividing the sub-volume, we have to make sure the partitions of the shared faces are consistent from both sides. This is achieved by a two-step partition strategy. The first step is to divide the sub-
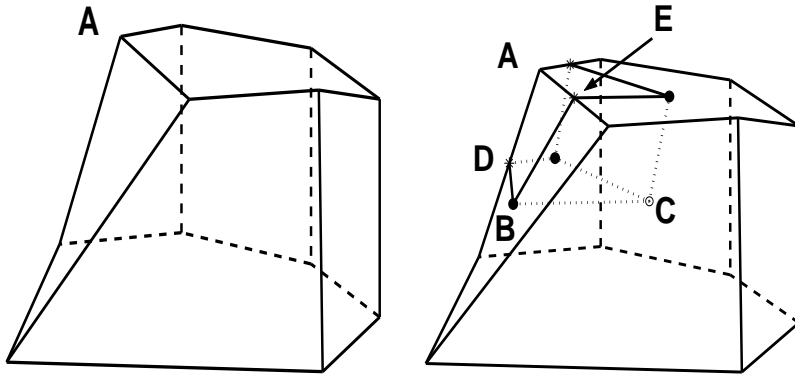
Figure 17: Polyhedral mesh. Left: A control volume; Right: The corresponding sub-volume.
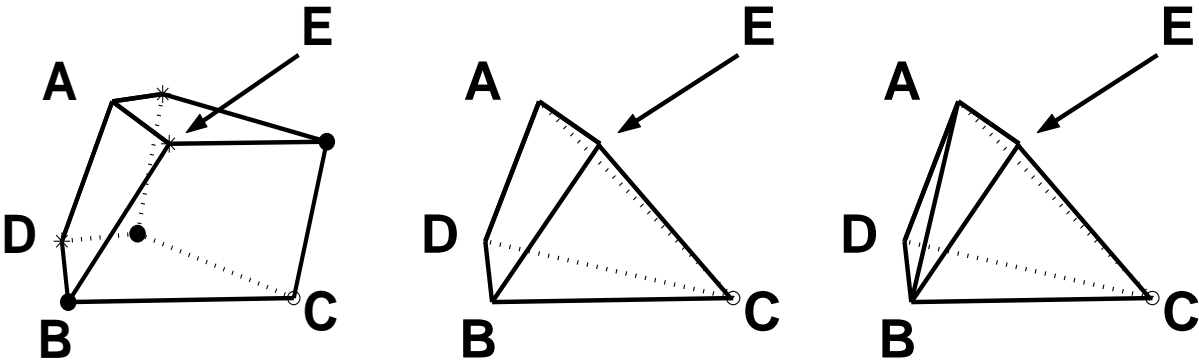

Figure 18: Polyhedral mesh: construction of local mesh.

volume into pyramids by connecting C with all the edge centers. One such pyramid is shown in the middle part of Fig. 18. The total number of pyramids is equal to the total number control volume faces which share point A. The second step is to partition each pyramid into two tetrahedrons by connecting point A to one previously computed face center which lies on the bottom of the pyramid (point B in Fig. 18). The resultant two tetrahedrons, $CABE$ and $CABD$, are shown in the right graph of Fig. 18. After all these, each interaction region is divided into non-overlapping tetrahedrons, on which a piecewise pressure can be defined.

4.2   Computation of Flux

Using a piecewise linear approximation for p on the local tetrahedron mesh constructed in the last section, we can compute ∇p and the flux across the interfaces. Clearly the flux formulation will involve the values of p at point A, C, face and edge centers, among which we only want to keep in

our final numerical scheme the primary unknowns, the values of p at volume centers. Again, like the algorithm for polygon meshes, we can eliminate face center unknowns by balancing fluxes, and remove p_A by using the Finite Element Method to solve the original equation on each individual interaction region. So the only unknowns needing extra work are those which sit at control volume edge centers. Bear in mind these unknowns cannot be eliminated through the above local FEM solve because the edge centers are on the boundaries of the corresponding interaction region.

We propose to use least square and averaging to directly approximate the edge center unknowns by linear functions of volume and face center unknowns. In each sub-volume, we implement a least square method to find a linear p from its values at the volume and face centers. For the sub-volume given in Fig. 18, the least square fitting simply becomes a linear interpolation procedure as there are only three face centers. In general, the least square method is still necessary because there may be more than three faces of a control volume which meet at a single point.

From the obtained linear function, one can compute the values of p at all edge centers for every sub-volume. Since each edge center point belongs to more than one sub-volume, we use the average of the values from all the sub-volumes at that point as the final value. After the averaging, the value at any edge center is expressed as a linear function of unknowns sitting in volume centers and face centers of all the sub-volumes in the local interaction region.

Combining everything together, we have the enriched multi-point approximation methods as follows.

Algorithm 1 *(EMPFA)*

1. *For each vertex of the mesh, construct the interaction region and local mesh as described in Sec. 4.1.*

2. *Employ a piecewise linear approximation of p on the mesh built in the first step. Use this approximation to compute the flux on each interface from the control volumes on both sides.*

3. *Solve the original equation with the Finite Element Method on the interaction region for pressure at the 'center' of the interaction region.*

4. *In each sub-volume, apply least square method to find a linear function of p from its values at the volume center and face centers.*

5. *Express the value of p at every edge center in terms of its values at all the volume centers and face centers, by averaging the linear functions in the sub-volumes which contains this edge center point.*

6. *Use the formula obtained in Step 2 and 5 to eliminate the pressure at edge centers and interaction region center from the flux formulation.*

7. *Eliminate face center pressures by balancing fluxes from both sides on each interface. It leads to a flux formulation in terms of control volume center pressures only.*

8. *Apply finite volume method to solve the original equation with flux computed in Step 7. It gives a linear algebraic equation which then can be solved by standard solvers.*

4.3   Numerical Results

In this section, we solve Eq. (1) with the EMPFA method described in the last section. In particular, we consider two grids given in Fig. 19. These two are actually two-and-a-half dimensional grids in the sense that they are built by first constructing a two dimensional grid on XY-plane, and then projecting this areal mesh in Z-direction to each layer. Apparently, the areal mesh for the grids in Fig. 19 are quadrilateral and polygon mesh respectively. We also randomly perturb the grids in the vertical direction as

$$z = z + \Delta z \times r \times \text{rand}([-1, 1]), \qquad 0 < r < 0.5,$$

where Δz is the grid size and rand($[-1, 1]$) means a uniform random number from $[-1, 1]$. One should note the control volume faces can be non-planar after the random perturbation (see the left graph of Fig. 19).

We choose $2\frac{1}{2}$-D grids because our algorithm is initially developed for reservoir simulations and nobody in petroleum industry is really interested fully three-dimensional grids at this moment.
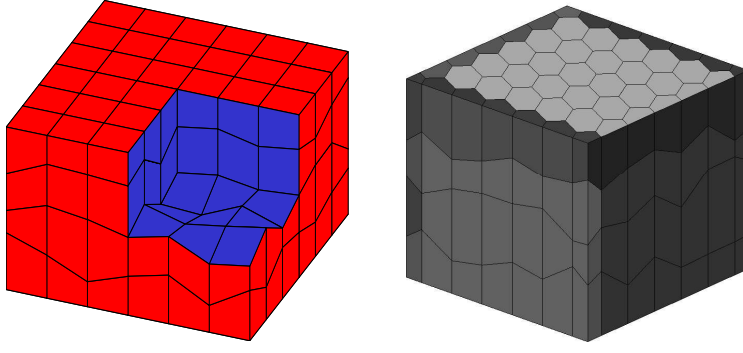
26

Figure 19: Two-and-a-half dimensional grids.

If not specified otherwise, we assume the domain is $[-1, 1]^3$, and the permeability takes the form

$$\mathbf{K} = \mathbf{O}_x^T \Lambda \mathbf{O}_x,$$

where $\Lambda = \text{diag}(10, 10, 1)$ and $\mathbf{O}_x$ is the rotation matrix around x-axis:

$$\mathbf{O}_x = \begin{pmatrix} 1 & 0 & 0 \\ 0 & \cos\theta & \sin\theta \\ 0 & -\sin\theta & \cos\theta \end{pmatrix}.$$

Problem 1 (Linear Flow) *Let the solution be*

$$p = x + y + z + 4.$$

The exact solution and flux are recovered for both meshes in Fig. 19 with random perturbation $r = 0.4$.

Problem 2 (Numerical Convergence) *Let the solution be*

$$p = \cos(\pi x) \cos(\pi y) \cos(\pi z).$$

The rotation angle is 30 *degrees and the perturbation parameter* $r = 0.3$.

When refining the mesh, we first refine the mesh uniformly in all the directions, and then perturb the z-coordinates, like all other random meshes. We compute the discrete L^2 error of pressure and normal flux which take the form

$$\begin{cases} ep & = \left(\sum_i |V_i| \, (p_{ex,i} - p_i)^2 \right)^{1/2}, \\ eu & = \left(\sum_{e \in \mathcal{E}} Q_e \left(\frac{f_{ex,e} - f_e}{|e|} \right)^2 \Big/ \sum_{e \in \mathcal{E}} Q_e \right)^{1/2}, \end{cases}$$

27

where $\{V_i\}$ is the set of all the control volumes and $\mathcal{E}$ is the set of all the control volume faces. $|V_i|$ denotes the volume of control volume V_i, while Q_e is the volume associated with face e. In this paper, the sum of the area of sub-volumes sharing face e is used as Q_e. The similar discrete error measures is used in Sec. 3.4.

We also compute the $H(div)_h$ error for the flux, defined as

$$\|\mathbf{u} - \mathbf{u}_h\|_{H(div),h} = \left(\sum_{\text{all } V_i} \int_{\partial V_i} (\mathbf{u}_h \cdot \mathbf{n} + \mathbf{K}\nabla p \cdot \mathbf{n})^2 \, dl \right)^{1/2},$$

where u_h denotes the numerical flux. Note that the discrete $H(div)_h$ error is actually computed in the paper by applying certain quadrature rule to the above boundary integral. The results are listed in Tab. 3 and 4.

Table 3: Discrete norms of the error. Quadrilateral areal mesh. N: number of grid points in each direction.

N	ep	Rate	eu	Rate	$\|\mathbf{u} - \mathbf{u}_h\|_{H(Div,.)}$	Rate
2	0.1351		6.2790		11.0248	
4	0.0297	2.18	3.2825	0.94	7.7657	0.51
8	0.0072	2.05	1.4317	1.20	4.5238	0.78
16	0.0018	2.01	0.6645	1.11	2.8617	0.66

Table 4: Discrete norms of the error. Polygonal areal mesh. NCell: total number of control volumes.

NCell	ep	Rate	eu	Rate	$\|\mathbf{u} - \mathbf{u}_h\|_{H(Div,.)}$	Rate
18	0.0497		6.2519		12.8434	
100	0.0222	1.41	4.2373	0.68	10.6348	0.33
648	0.0068	1.90	2.2228	1.04	7.3477	0.59
4624	0.0019	1.92	1.1290	1.03	5.0205	0.58

Problem 3 (Horizontal Well) *The permeability* $\mathbf{K} = \mathbf{O}_x^T \Lambda \mathbf{O}_x$, $\Lambda = diag(1000, 1000, 1)$ *and the rotation angle is* 30 *degrees. Zero pressure is imposed as boundary conditions.*

For this problem, we assume the horizontal well penetrates three control volumes in the center of the computational domain. No well model is involved in the implementation. We simply fix the
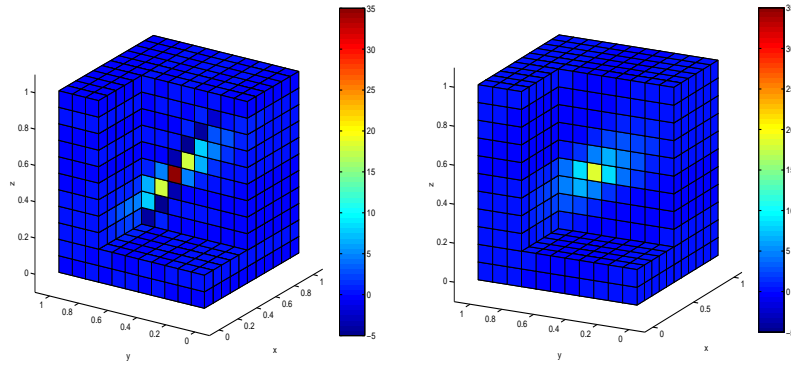
Figure 20: Pressure from MPFA and EMPFA. Left: MPFA; Right: EMPFA.

flow rate for each well block in the code, i.e.,

$$f(x, y, z) = \begin{cases} c & (x, y, z) \in \text{ well block,} \\ 0 & \text{otherwise,} \end{cases}$$

where c is some constant. The pressure profile is plotted in Fig. 20. Clearly, the solution from the enriched multi-point flux approximation method does not have the non-physical oscillations appearing in the MPFA solution.

5 Summary

The control volume multi-point flux approximation produces oscillatory solutions for diffusion processes in strongly anisotropic media. Within the setting of reservoir simulation, we showed that the oscillations are related to the poor approximation of pressure gradient in flux computation when the second order cross partial derivative of pressure is large. We then developed a new multi-point flux approximation, called enriched multi-point flux approximation (EMPFA), for general polygonal grids including non-matching grids. It is based on a more consistent approximation of pressure, and does not produce oscillatory solutions for strongly anisotropic permeability field, in contrast to other existent schemes such as the multi-point flux approximation method. The expected convergence rate is achieved.

We extended the enriched multi-point approximation method to unstructured polyhedral grids. Besides getting non-oscillating solutions, the EMPFA can also recover the exact linear solution for grids with non-planar interfaces, and compute the scalar and flux unknowns respectively with a first and second convergence on meshes which have perturbations of order $O(h)$.
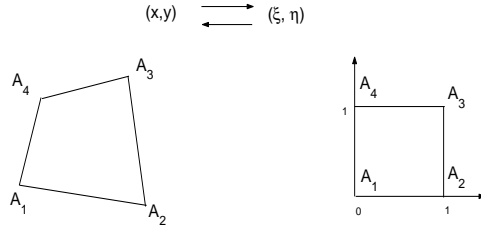
Acknowledgments

Figure A-1: From a quadrilateral to a reference element.

Appendix A   'Bilinear' Interpolation on Quadrilaterals

Here, we review the interpolation procedure of the quadrilateral element [12]. This interpolation is not an authentic bilinear interpolation on quadrilaterals. Instead, as shown in Fig. A-1, a quadrilateral $A_1A_2A_3A_4$ is mapped to a standard reference element, $[0,1] \times [0,1]$ in ξ-η plane, by a bilinear mapping with the form

$$
\begin{cases}
x &= x(\xi, \eta) = a_1 + a_2\xi + a_3\eta + a_4\xi\eta, \\
y &= y(\xi, \eta) = b_1 + b_2\xi + b_3\eta + b_4\xi\eta.
\end{cases}
\tag{A-1}
$$

The interpolated function is required to be bilinear on the reference element, i.e.,

$$
p(x, y) = p(\xi, \eta) = p_1 \, (1-\xi)(1-\eta) + p_2 \, \xi(1-\eta) + p_3 \, \xi\eta + p_4 \, (1-\xi)\eta,
$$

where $p_i = p_{A_i}, i = 1, \cdots, 4$, denote the values of the original function at point A_i's. The notation is abused a bit by using p to represent the interpolated function.

With simple computation, one can have

$$
\begin{cases}
a_1 = x_1, \\
a_2 = x_2 - x_1, \\
a_3 = x_4 - x_1, \\
a_4 = x_1 + x_3 - (x_2 + x_4),
\end{cases}
\qquad
\begin{cases}
b_1 = y_1, \\
b_2 = y_2 - y_1, \\
b_3 = y_4 - y_1, \\
b_4 = y_1 + y_3 - (y_2 + y_4),
\end{cases}
$$

where (x_i, y_i) is the coordinates of point A_i in x-y coordinate system. The Jacobian matrix of the mapping takes the form

$$
\mathbf{J} = \begin{pmatrix} \frac{\partial x}{\partial \xi} & \frac{\partial y}{\partial \xi} \\ \frac{\partial x}{\partial \eta} & \frac{\partial y}{\partial \eta} \end{pmatrix} = \begin{pmatrix} a_2 + a_3\eta & b_2 + b_4\eta \\ a_3 + a_4\xi & b_3 + b_4\xi \end{pmatrix}.
$$

So the gradient of the interpolated function at any point can be computed as

$$\begin{pmatrix} \frac{\partial p}{\partial x} \\ \frac{\partial p}{\partial y} \end{pmatrix} = \frac{1}{\det(\mathbf{J})} \begin{pmatrix} b_3 + b_4\xi & -(b_2 + b_4\eta) \\ -(a_3 + a_4\xi) & a_2 + a_4\eta \end{pmatrix} \cdot \begin{pmatrix} -(1-\eta) & 1-\eta & \eta & -\eta \\ -(1-\xi) & -\xi & \xi & 1-\xi \end{pmatrix} \cdot \begin{pmatrix} p_1 \\ p_2 \\ p_3 \\ p_4 \end{pmatrix}, \quad \text{(A-2)}$$

where $\det(\mathbf{J}) = (a_2 b_3 - b_2 a_3) + \xi(a_2 b_4 - b_2 a_4) + \eta(a_4 b_3 - b_4 a_3)$.

References

[1] SPE comparative solution project. http://www.spe.org/csp/datasets/set02.htm.

[2] I. Aavatsmark. An introduction to multipoint flux approximations for quadrilateral grids. *Computational Geosciences*, 6:405–432, 2002.

[3] I. Aavatsmark, T. Barkve, Ø. Bøe, and T. Mannseth. Discretization on non-orthogonal, curvilinear grids for multi-phase flow. In *Proc. of the 4th European Conf. on the Mathematics of Oil Recovery*, Røros, Norway, 1994.

[4] R. E. Bank and D. J. Rose. Some error estimates for the box method. *SIAM J.Numer. Anal.*, 24:777–787, 1987.

[5] M. Berndt, K. Lipnikov, J. Moulton, and M. Shashkov. Convergence of mimetic finite difference discretizations of the diffusion equation. *East-West J. Numer. Math.*, 9:253–316, 2001.

[6] M. Berndt, K. Lipnikov, M. Shashkov, M. Wheeler, and I. Yotov. Superconvergence of the velocity in mimetic finite difference methods on quadrilaterals. *SIAM J. Numer. Anal.*, 43(4):1728–174, 2005.

[7] F. Brezzi, K. Lipnikov, and M. Shashkov. Convergence of mimetic finite difference method for diffusion problems on polyhedral meshes. *SIAM J. Numer. Anal.*, 43(5):1872–1896, 2005.

[8] F. Brezzi, K. Lipnikov, and V. Simoncini. A family of mimetic finite difference methods on polygonal and polyhedral meshes. *Math. Models Methods Appl. Sci.*, 15:1533–1553, 2005.

[9] Z. Cai, J. Jones, , S. F. McCormick, and T. Russell. Control volume mixed finite element methods. *Computational Geosciences*, 1:289–315, 1997.

[10] Z. Cai, J. Mandel, and S. F. McCormick. The finite volume element method for diffusion equations on general triangulations. *SIAM J.Numer. Anal.*, 28:392–402, 1991.

[11] S.-H. Chou, D. Y. Kwak, and K. Y. Kim. A general framework for constructing and analyzing mixed finite volume methods on quadrilateral grids: The overlapping covolume case. *SIAM J. Numer. Anal.*, 39(4):1170–1196, 2001.

[12] P. G. Ciarlet. *The Finite Element Method for Elliptic Problems*. SIAM Classics in Applied Mathematics, Philadephia, PA, 2002.

[13] L. J. Durlofsky. Accuracy of mixed and control volume finite element approximations to darcy velocity and related quantities. *Water Resources Research*, 30(4):965–973, 1994.

[14] M. Edwards and C. Rogers. A flux continuous scheme for the full tensor pressure equation. In *Proc. of the 4th European Conf. on the Mathematics of Oil Recovery*, Røros, Norway, 1994.

[15] G. Eigestad and R. Klausen. Convergence of the MPFA O-method: Numerical experiments for discontinu ous media. *Numerical Methods for Partial Differential Equations*, 21(6):1079–1098, 2005.

[16] H. Hægland, H. Dahle, F. Eigestad, K.-A. Lie, and I. Aavatsmark. Improved streamlines and time-of-flight for streamline simulation of irregular grids. *Adv. Water Resour.*, 2006. submitted for publication.

[17] Z. Heinemann and C. Brand. Gridding techniques in reservoir simulation. In *First and Second International Forum on Reservoir Simulation*, Alpbach, Austria. September 12-16, 1998 and September 4-8, 1989, 339-426.

[18] R. Klausen and T. Russell. Relations among some locally conservative discretization methods which handle discontinuous coefficients. *Computational Geosciences*, 8(4):341–377, 2004.

[19] R. A. Klausen and R. Winther. Convergence of multi point flux approximations on quadrilateral grids. *Numerical Methods for Partial Differential Equations*, 22(6):1438–1454, 2006.

[20] Y. Kuznetsov and S. Repin. New mixed finite element method on polygonal and polyhedral meshes. *Russian Journal of Numerical Analysis and Mathematical Modeling*, 18(3):261–278, 2003.

[21] S. H. Lee, H. A. Tchelepi, P. Jenny, and L. J. Dechant. Implementation of a flux-continuous finite-difference method for stratigraphic hexahedron grids. *SPE Journal*, 7(3):267–277, September 2002. SPE paper 80117.

[22] S. F. Matringe, R. Juanes, and H. A. Tchelepi. Robust streamline tracing for the simulation of porous media flow on general triangular and quadrilateral grids. *Journal of Computational Physics*, 2006. In press.

[23] M. Mlacnik, L. Durlofsky, R. Juanes, and H. Tchelepi. Multipoint flux approximations for reservoir simulation. Presented at 12th Annual SUPRI-HW Affiliates Meeting, Stanford University, November 18-19 2004.

[24] R. L. Naff, T. F. Russell, and J. D. Wilson. Shape functions for velocity interpolation in general hexahedral cells. *Computational Geosciences*, 6(3-4):285–314, 2002.

[25] J. M. Nordbotten and I. Aavatsmark. Monotonicity conditions for control volume methods on uniform parallelogram grids in homogeneous media. *Computational Geosciences*, 9(1):61–72, 2005.

[26] J. M. Nordbotten and G. T. Eigestad. Discretization on quadrilateral grids with improved monotonicity properties. *Journal of Computational Physics*, 203:744–760, 2005.

[27] B. Rivière, M. F. Wheeler, and K. Banaś. Part II. discontinuous Galerkin method applied to a single phase flow in poros media. *Computational Geosciences*, 4(4):337–349, December 2000.

[28] H. Royden. *Real Analysis*. MacMillan, New York, NY, 1988.

[29] T. Schmidt. Box schemes on quadrilateral meshes. *Computing*, 51:271–292, 1993.

[30] M. Shashkov and S. Steinberg. Solving diffusion equations with rough coefficients in rough grids. *Journal of Computational Physics*, 129:383–405, 1996.

[31] S. Verma and K. Aziz. A control volume scheme for flexible grids in reservoir simulation. In *SPE Reservoir Simulation Symposium*, Dallas, Texas, 8-11 June 1997. SPE 37999.

[32] X. Wu and R. Parashkevov. Effect of grid deviation on flow solutions. In *SPE Reservoir Simulation Symposium*, Houston, Texas, 31 January - 2 February 2005. SPE 92868.